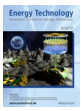

ZnS:Cu Phosphor Layers as Energy Conversion Materials for Nuclear Batteries: A Combined Theoretical and Experimental Study of Their Geometric Structure

Zhiheng Xu,[a] Xiaobin Tang,*[a, b] Yunpeng Liu,[a, b] Zhengrong Zhang,[a] Wang Chen,[a] Zicheng Yuan,[a] and Kai Liu[a]

The feasibility of utilizing the method of phosphor layer structure optimization to improve the performance of beta-radioluminescent nuclear batteries is investigated. The designs of different V-groove structures and conventional planar structures of ZnS:Cu phosphor layers are discussed. Monte Carlo simulations have been used to analysis the transportation of beta-particles released from the ^{63}Ni and ^{147}Pm plate sources, along with the corresponding energy deposition in the phosphor layers. Radioluminescence properties are characterized and the influence of configuration parameters on the luminescence intensity and emission wavelength is revealed. The current–voltage characteristic curves of beta-radioluminescent nuclear batteries with the above phosphor layer structures are used to analyze the electrical properties. Additionally, the deposited energy in the phosphors and radioluminescence luminous flux as a linear function of the maximum output power are investigated for different combinations of those phosphor layers and beta sources.

Introduction

As a type of nonthermal and indirect converter nuclear battery, even in the development phase, the beta-radioluminescent nuclear battery appears to be attractive for military applications, particularly for long-term and ultralow power applications. Beta-radioluminescent nuclear batteries are beta-decay-powered batteries that could potentially last for a long time and use phosphorescent materials to convert radiation into photons, which then impinge on a photovoltaic array.[1–3] The phosphors and semiconductors, as conventional radioluminescent and photovoltaic conversion materials, are of considerable interest both theoretically and technologically.[4–7]

A ZnS:Cu phosphor layer and a p–n junction gallium arsenide semiconductor were used as the radiation–luminescence–electricity converter. ZnS:Cu and GaAs materials have been typically and extensively studied for use in many fields, such as field-emission displays, optoelectronic devices, and power-supply applications.[7–9] They have also been reported to show high radioluminescence and photovoltaic conversion efficiency.[10–12]

For beta-radioluminescent nuclear batteries, the efficiency of energy conversion technologies is limited by their poor response to beta particles. One way of overcoming this limitation is to develop new materials and new methods that can efficiently convert kinetic energy from beta particles into electrical energy. Looking at the trends over the past decades, choosing one kind of suitable material and optimizing its structural design can achieve major improvements in output performance for an indirect conversion power supply device.[7,13] As the important energy conversion medium of the battery, structural optimization of the phosphor layers is critical to achieve higher efficiencies, especially for cases in which the battery materials have already been confirmed.

Thus, the motivation of this research is to study the potential effect of the phosphor layer geometry for beta-radioluminescent nuclear batteries. Herein, we show through theoretical calculations and experimental analyses that the geometric structure of the ZnS:Cu phosphor layers affects its energy deposition and luminescence transportation. A Monte Carlo simulation code was developed to simulate the radioactive decay of the radionuclide and its subsequent interaction with the phosphor layers. The emission and absorption of photons from ZnS:Cu phosphors and the resulting potential differences in the GaAs photovoltaic devices were analyzed. Two different beta radioisotopes, ^{63}Ni and ^{147}Pm, were selected as potential excitation sources. Specifically, the development of beta-radioluminescent nuclear batteries, prepared by adopting different structural parameters in their phosphor layers, and characterized under beta-particle excitation is presented.

[a] Z. Xu, Prof. X. Tang, Dr. Y. Liu, Z. Zhang, W. Chen, Z. Yuan, K. Liu
Department of Nuclear Science and Engineering
Nanjing University of Aeronautics and Astronautics
29 General Road, Jiangning District, Nanjing 211106 (P.R. China)
E-mail: tangxaiobin@nuaa.edu.cn

[b] Prof. X. Tang, Dr. Y. Liu
Jiangsu Key Laboratory of Material and
Technology for Energy Conversion
Nanjing 211106 (P.R. China)

Results and Discussion

Structure of the material and Monte Carlo simulations

A theoretical design and simulation of a beta-radioluminescent nuclear battery based on ^{63}Ni/^{147}Pm–ZnS:Cu was performed by using the Monte Carlo N-Particle Transport Code Version 5 (MCNP5) program. The purpose of this research is to study the interaction and mutual response between the beta sources and phosphor layers. The phosphor layer consists of two parts: an energy conversion part, consisting of a 16 μm thick phosphor powder, and a substrate made of a 29 μm thick adhesion layer. ZnS:Cu phosphors were directly adhered to the transparent adhesive tape with both high viscosity and high transparency. The V-groove structures of the ZnS:Cu phosphor layers were designed and prepared as presented in Figure 1. Dimension parameters h and θ of the different phosphor layers are listed in Table 1. Two beta-radioisotopes, ^{63}Ni and ^{147}Pm, were separately selected as potential excitation sources and subsequently modeled. To calculate the deposition energy in the ZnS:Cu phosphor layers, the full beta spectra were adopted in the theoretical models. Beta particles with a field radius of 1.5 cm were simulated as irradiating a projection area of 3 cm × 3 cm over the phosphor layer. Considering the alignment of beta-plate sources and phosphor layers, we have designed two extreme situations: Models A and B. Model A is represented as the center of the beta source and the bottom of the V-groove phosphor layers arranged in a line, whereas Model B is the top of the V-groove phosphor layers with the center of the beta source in alignment. For the same source and phosphor layer, the two models reflect the minimum and maximum relative offsets, respectively. Some simulation examples and partial enlarged details are shown in Figure 1c. Regardless of which structural system was adopted, the beta source was always placed directly on top of the phosphor powder layer and fitted closely together to form a whole during the simulation modeling and experimental measurement process.

The Monte Carlo approach was used herein to investigate the structural effects of the phosphor layers. The energy deposited by the beta particles was calculated in the ZnS:Cu phosphor layers. The number of simulated particles was 3×10^8, and the errors were all less than 0.05%. Figure 2 shows the deposited energy of the V-groove phosphor layers with different configuration parameters, as predicted by the simulation model. It can be seen that the energy deposition of the ZnS:Cu phosphors increases with decreasing angle θ within a certain height of phosphor layer. Analogously, the energy deposition also increases as the height h decreases for a given angle. This is mainly due to the configuration parameters h and θ, which are known to affect the phosphor powder concentration and radioluminescence transmission performance. Moreover, due to the stronger beta-particle energy, the deposited energy with the ^{147}Pm source is significantly higher than that with the ^{63}Ni source. However, for either ^{63}Ni or ^{147}Pm sources, the trends of the deposited

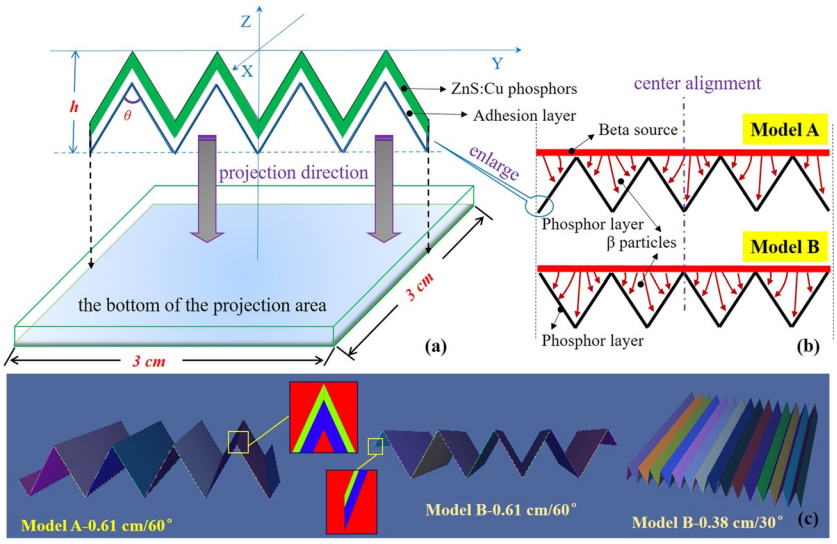

Figure 1. The MCNP model of the V-groove phosphor layers. a) Design and geometrical configurations of the material, with parameters h and θ. b) Two extreme alignments: Models A and B. c) A partial view of the simulation model.

Table 1. The configuration parameters of the V-groove phosphor layers.

Parameter	Values				
height h [cm]	0.38	0.41	0.61	0.81	1.01
angle θ [°]	30, 60, 90, 120, 150	30, 60, 90, 120, 150	30, 60, 90, 120	30, 60, 90, 120	30, 60, 90
projected area [cm^2]	9	9	9	9	9

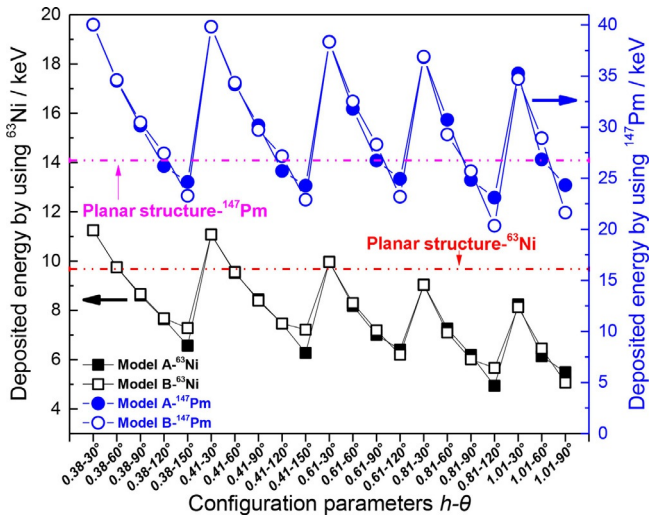

Figure 2. The beta-energy deposition is dependent on the configuration parameters of the V-groove phosphor layers.

energy changes with the configuration parameters of the V-groove phosphor layers are similar.

For comparison, the planar phosphor layers were introduced for comparison: the energy-deposition situation is shown in the inset of Figure 2. Because the competing effects of nuclear energy absorption and radioluminescence transmission were balanced and optimized, some V-groove phosphor layers were superior to the conventional planar structure under the same simulation conditions. Meanwhile, for different energy excitation sources, there was a significant difference, even if the same planar structure was adopted. Although the mean beta-particle energy of ^{147}Pm was 62.1 keV, still beyond that of ^{63}Ni with just 17.2 keV, according to the maximum penetration depth simulation results, a beta particle with the full-energy spectrum of the ^{63}Ni and ^{147}Pm components can travel with its maximum range inside ZnS:Cu phosphors to about 10.4 and 70 μm, respectively.[13] Considering the ranges of the ^{63}Ni beta particles and their penetration into the ZnS:Cu phosphor layer (about 10.4–16 μm; 16 μm is taken as the maximum particle energy) similar to the thickness of the phosphor powder used herein (16 μm), by contrast the planar structure shows some advantages over other structures. This is consistent with previous work, in which the V-groove increased the relative concentration of phosphors, but also increased the luminescence transmission distance. In addition, through a comparative analysis of the energy deposition in Models A and B, the gap between these two models was increasing with increasing angle, given the same excitation sources and height of the phosphor layers. Therefore, for this material, the size of the source and that of the phosphor layer have been confirmed. The relative displacement between them also deserves attention, especially when the included angle is larger.

The physical models of different V-groove phosphor layers were also established and analyzed under vacuum. The percentage of energy released by the beta source that was deposited into the ZnS:Cu phosphors were calculated. The results of different structures and combinations are given in Figure 3. A higher beta deposition energy was obtained for ZnS:Cu phosphors when analyzed in vacuum, rather than under atmospheric conditions; this is mainly because of the air-blocking effect. The beta-particle deposition and luminescence transmission situation were affected by the air gap between the beta source and the V-groove phosphor layer. For the ^{63}Ni source, which emits low-energy beta particles, the negative effect of air blocking was stronger than that of ^{147}Pm. Therefore, it can be seen from Figure 3 that the model with a ^{63}Ni source elicited a better performance in vacuo. It is speculated that putting the battery into a vacuum will be an efficient way to achieve a higher power output and enhance conversion efficiency for beta-radioluminescent nuclear battery designs in the future.

Radioluminescence properties of phosphor layers

The planar structure and different V-groove phosphor layers were prepared, as in the aforementioned simulation research. Unless otherwise noted, these samples were used for all subsequent tests. Radioluminescence, which is light emitted from ZnS:Cu phosphors immediately upon beta-particle irradiation, was measured at room temperature by using an electron-multiplying charge-coupled device (EMCCD) under 4.83 mCi cm^{-2} for ^{63}Ni and 1.36 mCi cm^{-2} for ^{147}Pm beta-plate sources. During the entire performance testing process, the relative position of the beta sources and phosphor layers was kept consistent in each combination. Radioluminescence imaging and testing of different V-groove phosphor layers were investigated, and some of the original images are shown in Figure 4. As can be seen from the photographs of the ^{63}Ni planar structure, the outline of the circular beta-plate source is clear and the luminescence is bright and vibrant.

Figure 5 shows the normalization of beta-radioluminescence optical imaging counts of the phosphor layers. There is a similarity with the trend of beta-particle energy deposited into the ZnS:Cu phosphors. The total counts of the optical imaging area of the phosphor layers decreased with increasing angle θ at a given height of phosphor layers. The total counts are also decreasing with increasing height h for a given angle. The trends were consistent with the theoretical analysis; however, it exhibited a different effect on the output performance when using two different sources, compared with the simulation results. Although the beta-particle average energy of the ^{147}Pm source is larger than that of the ^{63}Ni source, the activity density is much lower in comparison. The particle emergent performance of the ^{147}Pm source used in this experiment was significantly attenuated compared with the initial condition because of the very short half-life. However, the optical properties of the planar structure of the phosphor layers prepared with a beta-plate source offer a significant improvement over other V-groove configurations, through comparing the simulated and experimental results. The reason for the difference may be attributed to the positive optical transmission performance, especially when

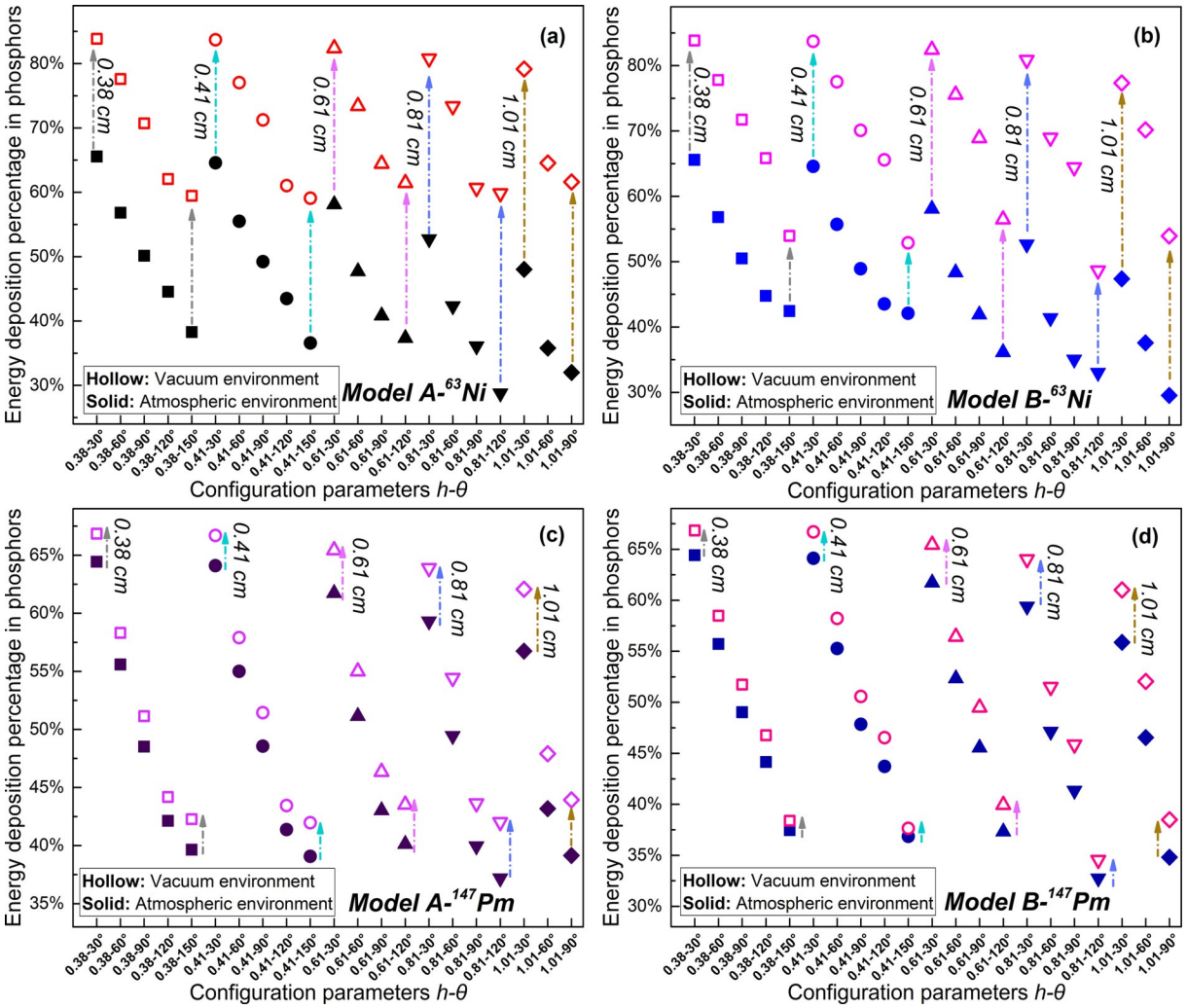

Figure 3. The beta-energy deposition percentage of beta particles deposited into the ZnS:Cu phosphors is dependent on the configuration parameters of the V-groove phosphor layers under different circumstances: a) for Model A and ^{63}Ni, b) for Model B and ^{63}Ni, c) for Model A and ^{147}Pm, and d) for Model B and ^{147}Pm.

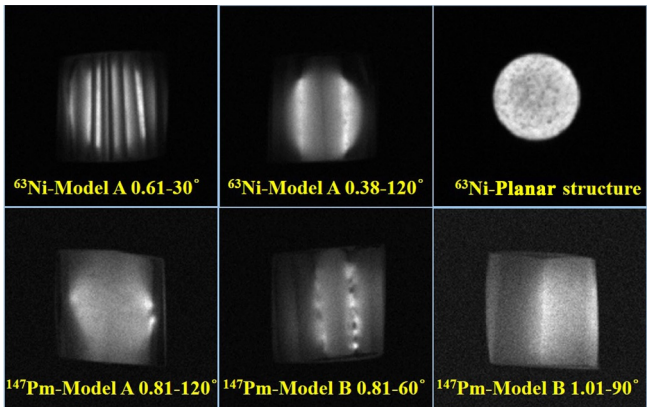

Figure 4. Photographs of different configurations of phosphor layers under excitation by different beta sources.

the thickness of the phosphor layer is similar to the penetration depth of beta particles in the phosphor materials.[4,13]

A calibrating system with customized 5.3“ integrating spheres was used to measure the optical output from the

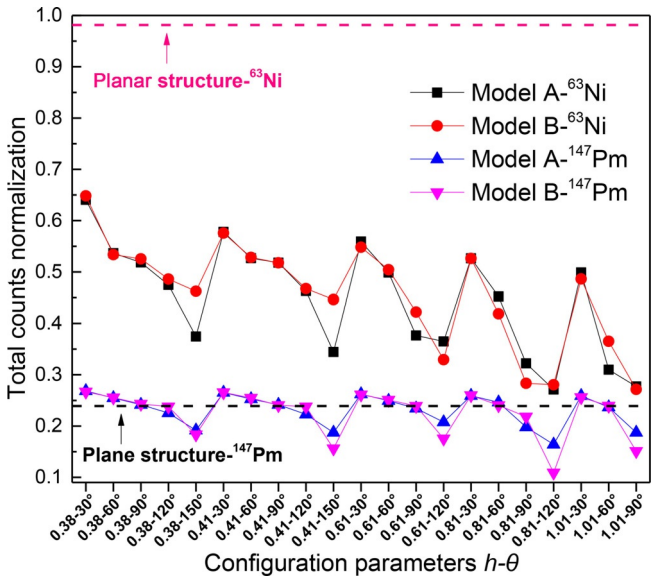

Figure 5. Normalized beta-radioluminescence optical imaging counts for phosphor layers with different configurations.

samples under the same beta sources. Figure 6 shows the layout of the experimental samples and testing equipment. The radioluminescence luminous flux was measured for the ZnS:Cu phosphor layers with different structures (Figure 7).

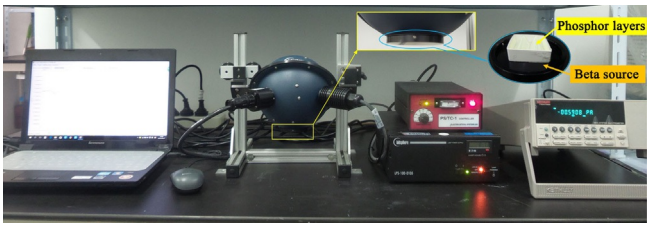

Figure 6. Radioluminescence luminous flux experimental test equipment.

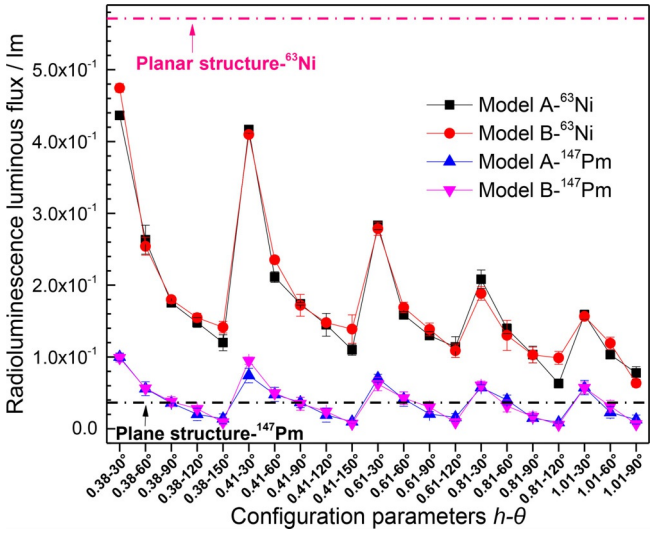

Figure 7. Radioluminescence luminous flux for phosphor layers with different configurations.

The luminous flux was increasing with decreasing angle θ for a given height, and it also increased with decreasing height h at a constant angle; a result consistent with the Monte Carlo simulation. The results indicate that greater energy deposition results in stronger radioluminescence light output within limits for the V-groove phosphor layers with a similar optical transmission mechanism. At the same time, an appropriate V-shaped groove structure can effectively improve the deposited energy per unit projected area, but the ability to improve light transmission performance is finite, relative to the conventional planar structure. Although the planar structure with the ^{147}Pm source deposited 2.6 times more energy as the ^{63}Ni variant, the ^{63}Ni source was about 3.55 times more active than the ^{147}Pm source. Similarly, for the same reasons, the radioluminescence properties of other structural phosphor layers with a ^{63}Ni source are generally superior to those structures with a ^{147}Pm source.

To assess the optical characterization, high-resolution radioluminescence spectra of different configuration phosphor layers were measured under excitation by the 4.83 mCi cm^{-2} ^{63}Ni and 1.36 mCi cm^{-2} ^{147}Pm beta sources (Figure 8). These samples had different radioluminescence intensities, which depended strongly on the type of beta source and geometric structure of the phosphor layers used, as in the previous experimental results. For different combinations of beta source and phosphor layer structures, the maximum emission wavelength was always maintained at $\lambda \approx 534$ nm, and the shapes of the radioluminescence spectra were similar. These results indicated that the configuration parameters of the phosphor layer influenced the optical output intensity, but had no interfering effect on the emission wavelength and spectral shape.

Electrical characteristics of beta-radioluminescent nuclear batteries

High-performance GaAs single-junction photovoltaic devices were used as energy-conversion units to absorb radioluminescence and to produce beta-radioluminescent nuclear batteries. Radioluminescent nuclear batteries are typically characterized through their electronic performance parameters (such as short-circuit current (I_{sc}), open-circuit voltage (V_{oc}), maximum output power (P_{max}), and fill factor (FF)). At the I_{sc} and V_{oc} points, the power will be zero and the maximum power will occur between the two. The voltage and current at this maximum power point are denoted as I_{mp} and V_{mp}, respectively. P_{max} is calculated by using Equation (1).

$$P_{max} = I_{sc}V_{oc}FF = MAX(IV) = I_{mp}V_{mp} \quad (1)$$

Figure 9 shows the change in P_{max} for different phosphor layer structures, as extracted from the measured current–voltage characteristic curves. The trends were similar to the radioluminescence optical performance test results: P_{max} increased as the angle θ or height h decreased, when another parameter remained the same. Based on the energy-conversion mechanism of the radioluminescent nuclear battery, it could be seen that, although the material type and effective action area of the photovoltaic device were identified and kept constant, the received luminescence became the key determinant. Herein, the maximum emission wavelength and spectral shape of the radioluminescence were almost constant. Therefore, the electrical output performance largely depends upon the radioluminescence intensity. The experimental results are in accordance with theoretical expectations.

The energy-conversion efficiency, η, of the beta-radioluminescent nuclear battery was determined as the fraction of beta particles emitted at power P_{source} that was eventually converted into electrical power [Eq. (2)]:

$$\eta = \frac{P_{max}}{P_{source}} = \frac{I_{mp}V_{mp}}{AE_{\beta}} = \eta_{\beta}\eta_{RL}\eta_{TR}\eta_{PV} \quad (2)$$

in which A is the source activity and E_{β} is the average energy of the beta source. Likewise, η is also reflected by the energy-transfer efficiency at each stage, in which η_{β}, η_{RL}, η_{TR},

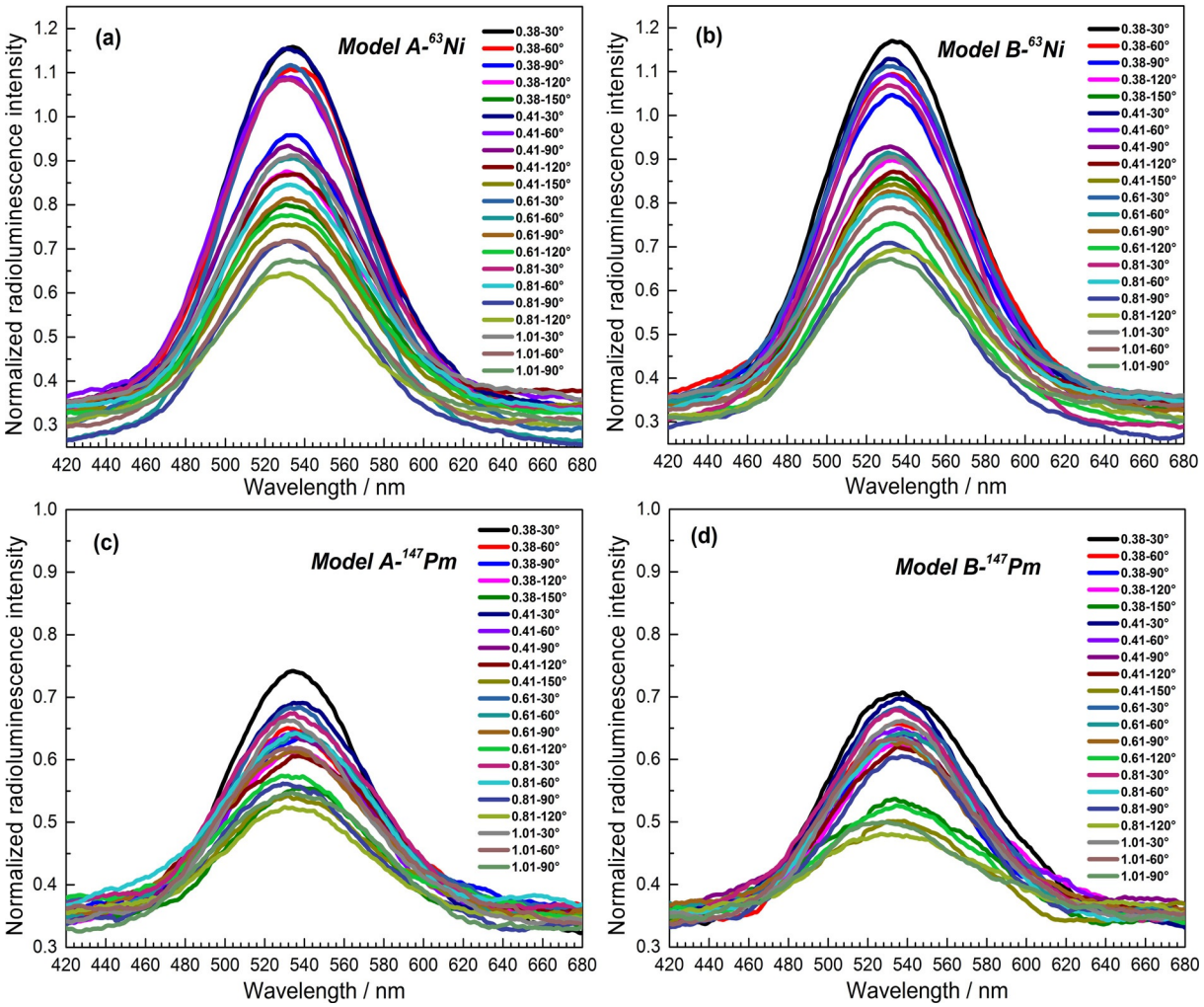

Figure 8. Normalized radioluminescence intensity of ZnS:Cu phosphor layers with different configurations under excitation by 4.83 mCi cm^{-2} ^{63}Ni and 1.36 mCi cm^{-2} ^{147}Pm beta sources.

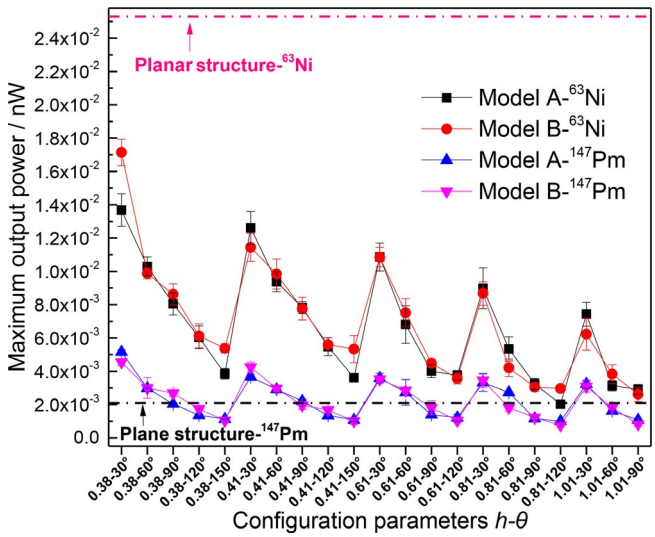

Figure 9. Maximum output power of beta-radioluminescent nuclear batteries with different configurations of phosphor layers.

and η_{PV} represent the conversion efficiency of beta-particle decay energy into useful energy deposition of the phosphor layer, the radioluminescence efficiency of beta-particle-deposited energy into luminescent energy, the transport efficiency of luminescence intensity from the phosphor layer to the surface of the GaAs photovoltaic device, and the photoelectric efficiency of the GaAs photovoltaic device, respectively.[14] The η values of the beta-radioluminescent nuclear batteries with different configurations of phosphor layers were calculated (Figure 10). The regularity of the changes reported herein, measured with various combinations, were consistent with the above results. The energy-conversion efficiency, η, of the planar phosphor layer structure was also measured for the previously mentioned ^{63}Ni source at 0.46% and for the ^{147}Pm source at 0.038%. If considering the actual energy-deposition situation, the effective η values will be higher. The energy-conversion process is influenced by various factors, including radiant particle release, luminescent transition, and charge collection efficiency.[15,16]

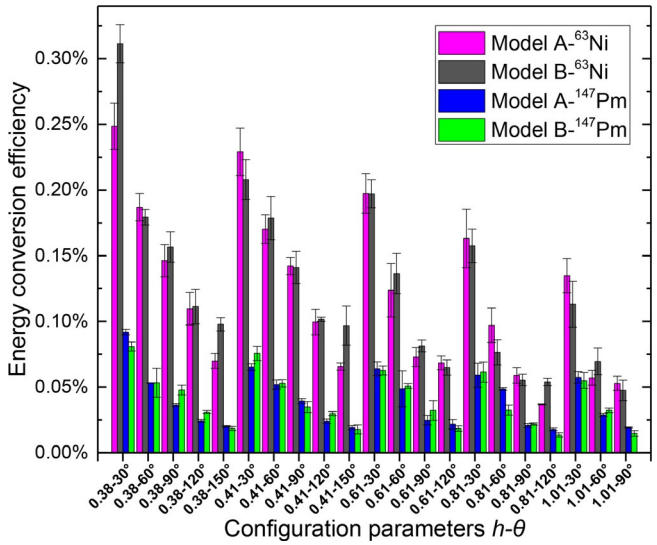

Figure 10. Energy conversion efficiency of beta-radioluminescent nuclear batteries with different configurations of phosphor layers.

In summary, the configuration parameters of the phosphor layers affect the output performance of beta-radioluminescent nuclear batteries. Therefore, designing a phosphor layer with suitable geometric parameters is an effective way to increase beta-particle deposition energy and improve the transmission of the emitted luminescence, especially when the materials used in the beta-radioluminescent nuclear battery are selected. In addition, as seen from the contrast between Models A and B (see Figures 9 and 10), the difference caused by the alignment of beta-plate sources and phosphor layers is apparent, so it is worthy of attention in the actual design process of this type of nuclear battery.

Relationship between deposited energy, radioluminescent intensity, and electrical performance

According to the theoretical simulation, and the radioluminescence and electrical performance test results, the structure of the phosphor layer was a crucial influencing factor. Further analysis of the results showed that those performance parameters may have an intrinsic relationship between them. The relationships between, and among, the beta-particle energy deposited into the ZnS:Cu phosphors, E_{dep}; the radioluminescence luminous flux, φ_{rad}; and the maximum output power, P_{max}, were correctly handled, as shown in Figure 11. The value of P_{max} of beta-radioluminescent nuclear batteries increased with increasing deposition energy, E_{dep}, and increased with increasing radioluminescence luminous flux, φ_{rad}. The significantly linear relationship between P_{max} and E_{dep}, and P_{max} versus φ_{rad} was achieved for four different combinations. The comparative analysis indicates that the initial MCNP5 simulation and optical measurement results can serve as a reliable predictor for reflecting the electrical output performance of the beta-radioluminescent nuclear batteries in future research.

Conclusions

The structural effect of the phosphor layer in a beta-radioluminescent nuclear battery has been investigated by theoretical simulations and experiments. The beta-particle deposited energy in ZnS:Cu phosphors for different structural systems was calculated and indicated that the deposition energy increased as the angle θ of the phosphor layer decreased, when the height h remained at a fixed value, and vice versa. Through optimization of configuration parameters, the V-groove phosphor layers can deposit more radiant energy than a conventional planar structure. In addition, the simulation showed that the energy deposition effect was improved, if the entire nuclear battery was placed in vacuo. A comparison between the two extreme alignments of the beta-plate source and phosphor layer revealed that the relative offset of both might also affect the output performance.

The radioluminescence optical imaging, radioluminescence optical properties, and current–voltage characteristic curves under excitation by the ^{63}Ni and ^{147}Pm beta-plate sources have also been used to measure the optical and electrical properties. The experimental values were shown to follow a similar trend to that of the calculated results. The absolute

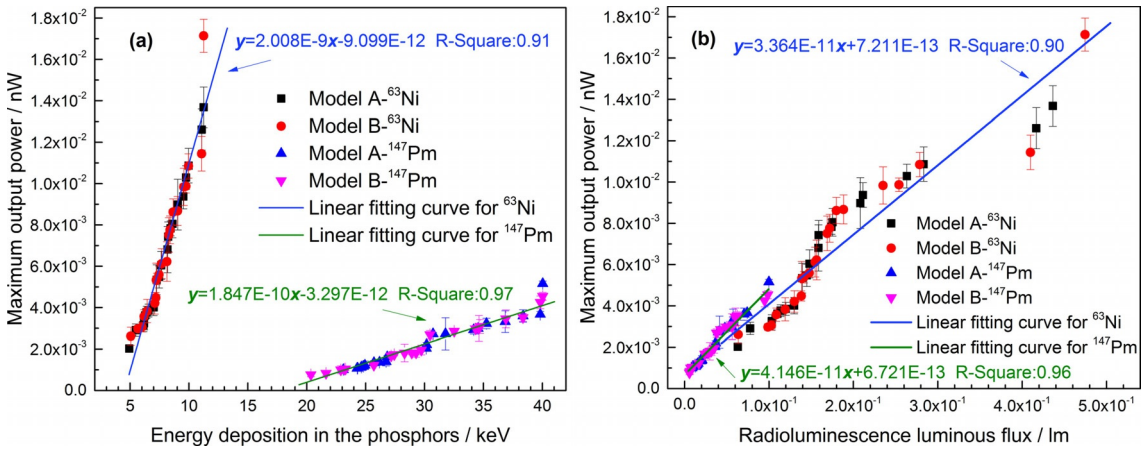

Figure 11. Plots of a) P_{max} versus E_{dep} and b) P_{max} versus φ_{rad} for phosphor layers with different configurations.

radioluminescent intensity and maximum output power of the combination with a ^{63}Ni source were greater than that of the combination with a ^{147}Pm source, which were related to the higher activity density. Although the excitation source and phosphor layer structure changed, the maximum emission wavelength and shapes of the radioluminescence spectra remained unchanged. Additionally, the deposition energy in the phosphors, the radioluminescence luminous flux, and the maximum output power all changed with similar tendencies to the configuration parameters of the phosphor layers. A linear relationship was found between the maximum output power and the deposition energy in the phosphors, as well as the radioluminescence luminous flux.

In summary, the results of simulations and experiments substantiate the feasibility of choosing optimized structural parameters to improve the output performance. According to all of the reported test results with ^{147}Pm as the irradiation source, the radioluminescence luminous flux of the optimum V-groove configuration was 2.74 times greater than that of the planar structure phosphor layer; furthermore, the maximum output power was 2.46 times higher than that of the planar structure. Thus, it cannot be thought of in such a simplistic way that the ultimate output performance of the optimized V-groove phosphor layers will definitely outperform the planar structure. During the design process of such types of nuclear batteries, each phase of energy exchange and conversion should be considered, such as the power deposition region of beta particles, the radioluminescence optical losses, the self-absorption effect, and proper coupling between the main components of the beta-radioluminescent nuclear battery.

Experimental Section

Optical property measurements

Radioluminescence was imaged by using an EMCCD camera (Andor iXon Ultra 888, USA) equipped with a Canon EF 24–70 mm f/2.8L II USM zoom lens. The integration time for all images was 30 s, the camera lens was Ø 82 mm, and the image resolution was 1024 × 1024 active pixels. The raw images were processed by subtracting a background image obtained under the same lighting conditions, but with the beta source removed. The camera was remotely controlled from outside the test chamber by a PC and a 20 m USB 3.0 extension cable. All light sources in the room were either turned off or blocked by a black sheet during the experiments. The reproducibility was tested by recording three consecutive images for each measurement and then calculating the standard deviation of each test result. The camera lens was mounted on a fixed bracket and placed at 0°, with respect to the incident radioluminescence, approximately 30 cm from the phosphor layers. The central position between the lens and phosphor layers was always consistent during each optical performance test. The camera and some test samples are shown in Figure 12.

The absolute intensity of the ZnS:Cu phosphor layers were characterized by using the Labsphere custom system and a Model 6514 system electrometer. The Labsphere custom light measurement system (CSTM-LMS-053-SL, USA) was composed

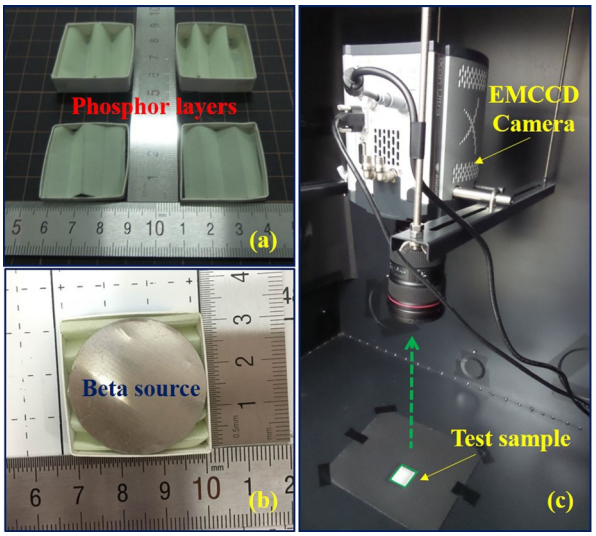

Figure 12. Photographs of a) the V-groove phosphor layers, b) the loading beta source, and c) the experimental setup for radioluminescence measurements.

of a custom 5.3“ spectralon sphere assembly, silicon detector (SCC-PM-SI), a TE-cooled detector controller (SDA-050-P-RTA-CX), a calibration lamp (LAB-SCL-050), and a power supply. The high-resolution radioluminescence spectra of the ZnS:Cu phosphor layers were measured on a Cary Eclipse luminescence spectrophotometer (Agilent Technologies G9800a, Malaysia), in which ^{63}Ni and ^{147}Pm were used separately as the sources and operated in bio-/chemiluminescence test modes.

Electrical property measurements

The current–voltage curve was measured on a dual-channel system source meter instrument (Keithley 2636A, USA), which provided valuable information about the *I–V* characteristics of beta-radioluminescent nuclear batteries.

All optical and electrical property tests were shielded from light and electromagnetic interference, and performed under identical room-temperature conditions. The method of multiple measurements and averaging was applied to ameliorate the effects of experimental error.

Acknowledgements

We acknowledge support received from the National Natural Science Foundation of China (grant nos. 11675076 and 11505096), the National Defense Basic Scientific Research Project (grant no. JCKY2016605C006), the Funding of Jiangsu Innovation Programme for Graduate Education (grant no. KYLX15_0302), and the Priority Academic Programme Development of Jiangsu Higher Education Institutions.

Conflict of interest

The authors declare no conflict of interest.

Keywords: energy conversion · luminescence · nuclear batteries · radiochemistry · structure–activity relationships

[1] X. B. Tang, Z. H. Xu, Y. P. Liu, M. Liu, H. Wang, D. Chen, *Energy Technol.* **2015**, *3*, 1121–1129.
[2] M. A. Prelas, C. L. Weaver, M. L. Watterman, E. D. Lukosi, R. J. Schott, D. A. Wisniewski, *Prog. Nucl. Energy* **2014**, *75*, 117–148.
[3] R. Walton, C. Anthony, M. Ward, N. Metje, D. N. Chapman, *Sens. Actuators A* **2013**, *203*, 405–412.
[4] C. D. Cress, C. S. Redino, B. J. Landi, R. P. Raffaelle, *J. Solid State Chem.* **2008**, *181*, 2041–2045.
[5] L. Hong, X. B. Tang, Z. H. Xu, Y. P. Liu, D. Chen, *Nucl. Instrum. Methods Phys. Res. Sect. B* **2014**, *338*, 112–118.
[6] Z. H. Xu, X. B. Tang, L. Hong, Y. P. Liu, D. Chen, *Nucl. Sci. Tech.* **2014**, *25*, 040603.
[7] K. E. Bower, Y. A. Barbanel, Y. G. Shreter, G. W. Bohnert, *Polymers, Phosphors, and Voltaics for Radioisotope Microbatteries*, CRC Press, Boca Raton, FL, **2002**, pp. 42–302.
[8] Non-solar photovoltaics for small space missions: G. A. Landis, S. G. Bailey, E. B. Clark, M. G. Myers, M. F. Piszczor, M. S. Murbach in *38th IEEE Photovoltaic Specialists Conference* (Texas, USA), **2012**, pp. 002819–002824.
[9] M. Sychov, A. Kavetsky, G. Yakubova, G. Walter, S. Yousaf, Q. Lin, D. Chan, H. Socarras, K. Bower, *Appl. Radiat. Isot.* **2008**, *66*, 173–177.
[10] H. Chen, L. Jiang, X. Chen, *J. Phys. D* **2011**, *44*, 215303–215306.
[11] M. Brossard, C. Y. Hong, M. Hung, P. Yu, M. D. B. Charlton, P. G. Savvidis, P. G. Lagoudakis, *Adv. Opt. Mater.* **2015**, *3*, 263–269.
[12] M. Prelas, M. Boraas, F. De La Torre Aguilar, J.-D. Seelig, M. T. Tchouaso, D. Wisniewski, *Nuclear Batteries and Radioisotopes, Lecture Notes in Energy, Vol. 56*, Springer, Cham, **2016**, pp. 105–240.
[13] Z. H. Xu, X. B. Tang, L. Hong, Y. P. Liu, D. Chen, *J. Radioanal. Nucl. Chem.* **2015**, *303*, 2313–2320.
[14] L. Hong, X. B. Tang, Z. H. Xu, Y. P. Liu, D. Chen, *J. Radioanal. Nucl. Chem.* **2014**, *302*, 701–707.
[15] S. Rahastama, A. Waris, *J. Phys. Conf. Ser.* **2016**, *739*, 012003.
[16] R. Y. Yu, S. Z. Jin, S. Y. Cen, P. Liang, *IEEE Photonics Technol. Lett.* **2010**, *22*, 1765–1767.

Manuscript received: January 17, 2017
Revised manuscript received: February 15, 2017
Accepted manuscript online: February 16, 2017
Version of record online: May 3, 2017

